

Near-Infrared Spectroscopic Sensing of Hydrogen Order in Ice XIII

Christina M. Tonauer^{1,†}, Eva-Maria Köck¹, Raphael Henn², Christoph Kappacher²,
Christian W. Huck², and Thomas Loerting^{1,*}¹*Institute of Physical Chemistry, University of Innsbruck, A-6020 Innsbruck, Austria*²*Institute of Analytical Chemistry and Radiochemistry, University of Innsbruck, A-6020 Innsbruck, Austria*

(Received 14 March 2024; accepted 15 May 2025; published 2 July 2025)

We identify hydrogen ordering in H₂O ices spectroscopically in the near-infrared (NIR) range (10 000–4000 cm⁻¹/1–2.5 μm) based on the example of ices V/XIII. Previously it was thought that hydrogen ordering can only be revealed on the basis of lattice phonons, i.e., intermolecular vibrations. Here we show differences in the overtone spectrum of the intramolecular OH-stretching vibration. This makes NIR spectroscopy the first remote sensing method that is sensitive to different orientations of the water dipoles within ice. As such it will allow for future observations of the hydrogen order of ices in space by the James-Webb Space Telescope or the JUICE mission.

DOI: [10.1103/x2ph-yp2v](https://doi.org/10.1103/x2ph-yp2v)

We here establish near-infrared spectroscopy (NIR) and overtones of intramolecular vibrations as a method for identification of hydrogen order using ices V/XIII as a benchmark case. The first OH-stretching overtone is a powerful marker for differentiating ordered and disordered H-atom networks of ices. This represents the first marker that is suitable for remote measurements on icy objects, thereby allowing access to dipolar orientation and hence mechanical and dielectric properties of ices in space, e.g., using the observations by the James-Webb Space Telescope (JWST) and Jupiter Icy Moons Explorer (JUICE).

Water in the solid state displays at least 20 different known forms of crystalline ice [1] and three different types of amorphous ice [2]. Many of these ices occur in remote places, such as interstellar clouds, the mantle of icy moons, or the interior of ice giants [3]. In essence, H₂O ices can be categorized based on order and disorder in the arrangement of oxygen atoms and hydrogen atoms. Disordered oxygen atoms define amorphous ices, while an ordered lattice of oxygen atoms defines crystalline ices. The crystalline ices are subdivided into low and high permittivity ices, where the former show order in the sublattice of hydrogen atoms and the latter feature random orientations of water dipoles, where the Bernal-Fowler ice rules [4] allow for six possible orientations. The arrangement of the H atoms in an ice has a huge impact on the electric properties,

such as ferroelectricity and antiferroelectricity [5–7], and also on the flow properties, such as superplasticity or diffusion creep [8,9].

The gold standard for laboratory identification of whether or not the sublattice is ordered is neutron diffraction on D₂O samples [10–23]. Owing to unfavorable cross sections for H₂O ice this technique is unsuitable for sensing of H ordering in samples of natural isotopic abundance. Also, x-ray diffraction is barely sensitive to the H atom positions, but mostly to the electrons surrounding the oxygen atoms. A second important method to infer order is calorimetry, which is also suitable for H₂O ices and used in our laboratory studies. A third method to probe for H order is Raman lattice mode spectroscopy, which is sensitive to the intermolecular arrangement in H₂O networks. Raman has been extensively used to study water ice [24–36], but mostly employed as a fingerprint method to probe for the network of oxygen atoms. There has only been a handful of Raman lattice mode studies, in which order-disorder has been distinguished, most notably for ices I_h/XI [30], ices III/IX [29], and ices V/XIII [31]. The very broad intramolecular OH-stretching and OH-bending vibrations are expected to be insufficient to probe differences between ordered and disordered ices because their structural differences, i.e., the orientations of water molecules, manifest on the intermolecular level [35,37]. None of these above-mentioned methods is suitable for remote sensing of H₂O ices on astronomical bodies. That is, a method enabling remote sensing of H order is still lacking. In the present Letter we demonstrate the capability of near-infrared spectroscopy to distinguish between H order and disorder based on the example of ices XIII and V, which we assume to be present on some icy moons.

For example, the Jupiter moon Ganymede is thought to consist of a ~800-km-thick water ice mantle, with

*Contact author: thomas.loerting@uibk.ac.at†Contact author: christina.tonauer@uibk.ac.at

concentric layers of ices I/III/V/VI [38] and a liquid subsurface ocean in between [39,40]. While ionic or carbonaceous impurities are practically insoluble in all these ices at < 1 GPa, the liquid layer is thought to contain dissolved ions (Na^+ , Mg^{2+} , SO_4^{2-} , Cl^-) that are remnants of chondrites accreting during the formation of the satellite [41]. The craters on the surface of Ganymede within bright high-albedo regions suggest cryovolcanic and tectonic activity [42]. Therefore, pure high-pressure ices from lower mantle regions, e.g., ice V at a ~ 500 km depth, may be carried together with liquid and/or solid brine lavas to the surface. At Ganymede's surface, daytime temperatures are ranging from ~ 90 K (near the poles) to ~ 160 K (near the equator) [38,43]. That is, at locations where temperatures are below the H-ordering temperature of 116 K [44], H ordering is favored. That means, after the transport from the interior to the surface, ice V will very slowly, over the years, transform to more and more ordered ice XIII at cold regions at the surface. While there is plenty of time for ordering to occur on astronomical timescales, there is usually not enough on laboratory time scales. The ordering typically takes weeks, months, or even years at < 120 K; therefore laboratory studies need to employ an intentional creation of defects by doping with ppm amounts of HCl as a strategy to achieve ordering on the timescale of hours and days. Salzmann *et al.* [11] first reported the ordering of deuterated and DCl doped ice V (space group $A2/a$) [12] at 0.5 GPa, resulting in ordered ice XIII ($P2_1/a$) [11]. Recently, a partly ordered intermediate between ice V and XIII has also been reported [45]. That is to say, while ice XIII can be made in the laboratory, direct detection in nature has remained elusive, even though surface temperatures of icy Jupiter and Saturn moons are low enough for H-ordered ices to be thermodynamically favored. Depending on the surface temperature at a specific geographic location [38,43], ice XIII ($< \sim 100$ K), ice V ($< \sim 130$ K), or stacking disordered ice I_{sd} (~ 130 – 160 K) [46] as well as ordinary ice I_h and XI [35,37] may be present on icy moons. That is, the identity of the ice phases observed is a probe for current and past surface temperatures. At the poles of Ganymede the highest daytime temperatures do not exceed 90 K so that we assume slow conversion of surfaced ice V to ice XIII both in the daytime and nighttime. The insolubility of almost all substances in ice means that we expect observations in nature that are rather similar to our laboratory observations on pure ices. The only substances that are soluble (up to the ppm level) in ice are small acids and bases such as HCl and KOH that usually accelerate the ordering transition by producing point defects in the ice lattice [47]. As of now, however, it is unclear whether disordered ice V or ordered ice XIII is encountered in astrophysical environments such as on Ganymede. This is in part because of a hiatus of infrared spectroscopy studies on ice polymorphs after the pioneering works of Whalley and coworkers on ices I–VI in the

1960s [48–54]. Back then, no H-order or H-disorder ice pairs were available for comparison, and after their discovery infrared spectroscopy of ices was neglected. In recent years, however, there has been a renaissance of infrared spectroscopy for exploring the physics of water ices. This is due to the development of new experimental techniques such as multidimensional coherent IR spectroscopy for probing dynamics [55–61] in combination with advanced computational methods for the interpretation of the vibrational signatures [61–68]. For remote sensing, the launches of the JWST that is equipped with the Near Infrared Spectrograph (NIRSpec) operating in the range 0.6– $5 \mu\text{m}$ and the Jupiter Icy Moons Explorer with the MAJIS instrument (0.4– $5.7 \mu\text{m}$) [69] have pushed the field and triggered our efforts to provide high-quality laboratory reference spectra of ices in the mid- and near-infrared range.

In our previous work, we presented the NIR spectra ($10\,000$ – $4\,000 \text{ cm}^{-1}$ /1– $2.5 \mu\text{m}$) of (H_2O) high-pressure ices II, IV, V, VI, IX, and XII [70]. All of these ices differ in terms of the arrangement of oxygen atoms in the lattice as well as their density. We observed that especially the first overtone band of the OH-stretching vibration ($2\nu_{\text{OH}}$) with its shoulder ($\sim 6050 \text{ cm}^{-1}$ /1.65 μm in the case of ice I_h) is a strong marker for ice polymorphs, showing a blueshift with increasing density [70]. Even though there are ordered and disordered ices among the ones studied earlier by us [70], we have not provided evidence for the possibility of identifying H-order using NIR spectroscopy. Here we present a direct comparison of spectra for the H-disorder and H-order pair (H_2O) ice V/ice XIII and show that H order can be identified in the NIR spectrum of ice XIII. This finding establishes that the vibrational overtone spectrum does not only indicate structural differences between ice phases with distinct oxygen networks and density, but is even sensitive to different orientations of the water molecules. In addition to the relevance for remote sensing our Letter also bears fundamental implications for our understanding of e.g., anharmonicity of OH vibrations in hydrogen-ordered ices.

Three separate batches of ice XIII were prepared in a custom-made high-pressure piston-cylinder setup [71] following the p - T protocol described in Ref. [11]. More specifically, for one batch, 600 μl of 0.01 M HCl in an indium container were compressed to 0.5 GPa at 77 K and subsequently heated to 250 K, yielding the expected polymorphic transition sequence ice $I_h \rightarrow \text{III/IX} \rightarrow \text{II} \rightarrow \text{ice V}$ [44]. The sample was then cooled, below 140 K at a cooling rate of 0.7–0.9 K min^{-1} , allowing for the hydrogen-ordering transition to ice XIII to occur. At 77 K, the samples were decompressed to ambient pressure and recovered. Batches of ice V were produced in a similar way, but using pure H_2O instead of 0.01 M HCl and by applying fast cooling rates by quenching with liquid nitrogen [70]. Omitting the dopant HCl slows down the ordering dynamics by orders of magnitude so that no

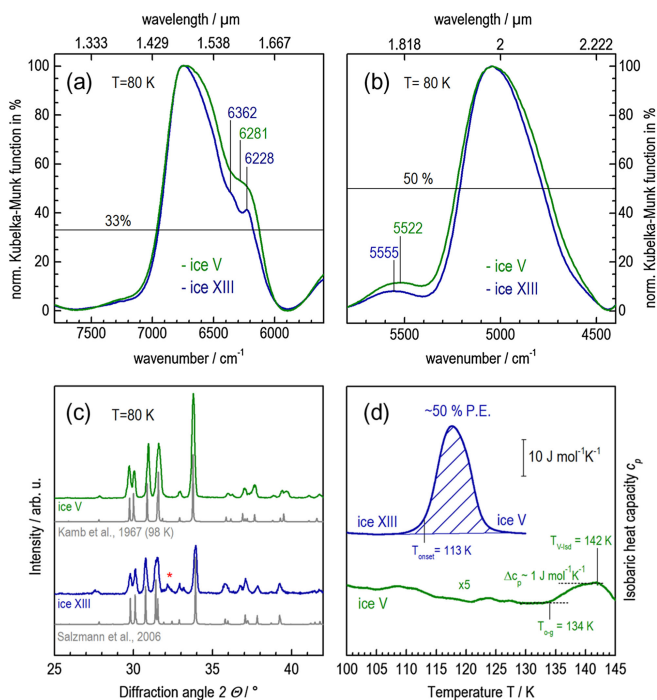


FIG. 1. Near-infrared spectrum of ice XIII (blue) in comparison with ice V (green, [70]) in the range of (a) the $2\nu_{\text{OH}}$ and (b) the 5000 band. We used a Büchi NIR Flex N-500 benchtop spectrometer in diffuse reflectance mode for collecting spectra of powdered samples at ~ 80 K and ambient pressure in the range of $10\,000\text{--}4000\text{ cm}^{-1}$ ($1\text{--}2.5\text{ }\mu\text{m}$). Nineteen (cumulative) high-quality reflectance spectra were collected and converted to the Kubelka-Munk (K-M) spectra [70]. Baseline correction was executed by subtraction of a basis spline function (constructed from eight anchor points) from the raw spectra (provided in the Supplemental Material [72]). The corrected spectra were then normalized with respect to the $2\nu_{\text{OH}}$ maximum, summed up, and are shown in (a),(b) and in Fig. S1 of the Supplemental Material [72], scaled to the maximum of the chosen band (100% K-M). (c) Powder x-ray diffractograms of ice V and ice XIII collected in $\theta\text{--}\theta$ geometry at ~ 80 K and 1 mbar (Cu-K α ; Siemens D5000), with the respective literature diffractograms below [11,12]. (d) DSC heating scans of a sample of ice XIII, showing the endothermic H order-to-disorder transition (onset temperature 113 K) and of a sample of H-disordered ice V, showing no such transition, but only the orientational glass transition at higher temperature ($T_{o-g} = 134$ K). The degree of H order is indicated as a percentage of Pauling entropy (PE), i.e., $3.37\text{ J mol}^{-1}\text{ K}^{-1}$ [44]. Each batch of ice XIII was characterized by heating samples of $\sim 10\text{--}20$ mg in aluminum crucibles from ~ 93 K to ~ 130 K at 10 K min^{-1} using a DSC8000 by Perkin Elmer. For baseline correction, a heating scan of the sample—after *in situ* transformation to ice I_{h} —was subtracted from the raw scan. The thermograms are normalized by the melting enthalpy of ice I_{h} (6012 J mol^{-1} at 273 K). Temperatures are within an uncertainty of ± 1 K.

ice XIII forms upon cooling, especially upon rapid cooling [47]. For the NIR characterization we applied the diffuse scattering method established previously [70]

[Figs. 1(a) and 1(b)]. The ice polymorph was confirmed by powder x-ray diffraction (PXRD) [Fig. 1(c)], and the degree of H order in ice XIII was assessed using differential scanning calorimetry (DSC) [Fig. 1(d)].

In Figs. 1(a) and 1(b) the two strongest features in the near-infrared spectrum of ices V (green, from Ref. [70]) and XIII (blue) are highlighted: (a) the first overtone band of the OH-stretching vibration ($2\nu_{\text{OH}}$) around $\sim 6740\text{ cm}^{-1}$ and (b) the combinational band of the OH-stretching with the bending mode or first overtone of the libration mode ($\nu_{\text{OH}} + \nu_2/\nu_{\text{OH}} + 2\nu_{\text{R}}$) around $\sim 5000\text{ cm}^{-1}$ (for simplicity, “5000-band”). The combination of both PXRD and DSC [Figs. 1(c) and 1(d)] is necessary for an unambiguous differentiation. While PXRD probes the oxygen lattices (which are very similar in the case of order-disorder pairs), DSC probes changes in heat capacity and release and uptake of heat upon heating, disclosing the presence or absence of H order. In the powder x-ray diffractogram [Fig. 1(c)] of ice XIII, H order is indicated by the presence of a weak Bragg peak $\sim 32.2^\circ$ (marked by a red asterisk) which is absent in ice V [11,47], in agreement with the literature [11,12] (gray). Differences in peak intensities solely result from texture effects, i.e., preferred orientations within the powdered grains, typical for PXRD in $\theta\text{--}\theta$ geometry [47].

The degree of H order was measured by DSC scans at a heating rate of 10 K min^{-1} [Fig. 1(d)]. Ice XIII shows an endothermic peak with onset temperature T_{onset} of 113 K, slightly higher than the one observed in Ref. [44] (110 K, heating at 5 K min^{-1}). The area of the H-disordering endotherm (marked by dashed lines) divided by T_{onset} results in the entropy gain accompanied by the disordering transition [given as % Pauling entropy (PE)]. We here consider samples of $\sim 50\%$ PE (where the maximum was reported to be 66% [44]). The degree of H order as well as T_{onset} critically depend on the sample preparation and thermal history. This includes the cooling rate of HCl doped ice V at 0.5 GPa, the storage time in a liquid nitrogen dewar [73], and the heating rate during calorimetry at ambient pressure. The DSC scan of ice V [Fig. 1(d)] expectedly shows no H-disordering endotherm. At 134 K, we observe the orientational glass transition T_{o-g} ($\Delta c_p \sim 1\text{ J mol}^{-1}\text{ K}^{-1}$), followed by the ice V \rightarrow ice I_{sd} transition (~ 142 K). The slight differences compared to the values in the literature (T_{o-g} : 130 ± 1 [73], ~ 132 K [44]; Δc_p : 1.7 ± 0.2 [73], $3.7\text{ J mol}^{-1}\text{ K}^{-1}$ [44]) result from different preparation conditions (i.e., ice V prepared by quenching at 0.64 GPa [73] and slow cooling at 0.5 GPa [44] versus quenching at 0.5 GPa) and different calorimetric protocols (i.e., heating rate 30 [73] and 5 [44] versus 10 K min^{-1} as presented here).

The key findings in the present Letter are the spectra in Figs. 1(a) and 1(b), where the most obvious spectral difference between ice XIII and ice V is the low-wave number shoulder of the $2\nu_{\text{OH}}$ band. While this feature is a

broad shoulder for ice V at 6281 cm^{-1} , there is a clear splitting of this feature in ice XIII, showing subpeaks at 6362 and 6228 cm^{-1} , respectively (Table I). This is the spectroscopic signature of hydrogen order in ice XIII. To the best of our knowledge, the mid-infrared spectrum of H_2O ice XIII containing the fundamental OH-stretching band has not been reported yet. However, Tran *et al.* measured the OD-stretching band at $2300\text{--}2600\text{ cm}^{-1}$ for D_2O ices V and XIII (Fig. 3C in Ref. [56]). On a qualitative level, the line shape of the $2\nu_{\text{OH}}$ shoulder in Fig. 1(a) resembles the ν_{OD} feature shown by Tran *et al.* [56]. That is, their spectrum of D_2O ice V shows a broad plateaulike band with three shallow subpeaks. This is in agreement with our previous finding of three subpeaks within the broad $2\nu_{\text{OH}}$ shoulder [70]. This can be seen best in the first derivative of the spectrum; see Fig. S2 in the Supplemental Material [72], and Table I. On the other hand, their D_2O ice XIII spectrum shows two strong subpeaks (at 2410 and 2513 cm^{-1} [56]) and more substructure, very similar to the overtoneband presented here [Fig. 1(a)].

Furthermore, we find band width in the NIR spectrum to be a marker for H order. The two strongest bands of ordered ice XIII show significant narrowing relative to the disordered counterpart ice V [Figs. 1(a) and 1(b)]. Owing to the asymmetric shape of the $2\nu_{\text{OH}}$, we use the measure full width at one third of the maximum (FWTM) [70] for its broadness which decreases by 59 cm^{-1} in ice XIII. Similarly, the FWHM of the 5000 band decreases by

TABLE I. Band positions and width/intensity for three NIR bands of ices V and XIII in comparison. FWTM and FWHM are used as measures for peak width of the $2\nu_{\text{OH}}$ and the 5000 band, respectively.

Ice V [70]	Ice XIII	
$2\nu_{\text{OH}}/\text{cm}^{-1}$		
6746	6740	Maximum
	6362	Shoulder (see Supplemental Material, Fig. S2 [72])
6311		
6281		
6253	6228	
$\text{FWTM}/\text{cm}^{-1}$		
835	776	Δ/cm^{-1} 59
$\nu_{\text{OH}} + \nu_2 + \nu_{\text{R}}/\text{cm}^{-1}$		
5522	5555	Δ/cm^{-1} 33
Intensity (relative to 5000 -band) in %		
12	8	
$5000\text{ band}/\text{cm}^{-1}$		
5043	5044	
$\text{FWHM}/\text{cm}^{-1}$		
482	434	Δ/cm^{-1} 47

47 cm^{-1} (Table I). Arakawa *et al.* claim a similar effect of H order on band width for the ice I_h /ice XI pair. They consider narrowing of the librational band (ν_{R}) at $\sim 850\text{ cm}^{-1}$ [35,37], and assign a discontinuous change of band width below 140 K to H ordering in ice I_h , while the (thermodynamic) H-ordering transition of ice $\text{I}_h \rightarrow$ ice XI actually occurs at 72 K [74]. That is to say, Arakawa *et al.* find signatures for nonthermodynamic, local, or kinetic H ordering in their $2\text{ }\mu\text{m}$ thin ice samples sandwiched between diamond windows. This ferroelectric H ordering might be restricted to the first few monolayers at the ice surface, consistent with the study by Sugimoto *et al.* [75]. It might also be kinetically trapped domains in the bulk, as suggested by Arakawa *et al.* themselves [76]. Also irradiation of the sample may trigger local ordering above 72 K in the near-surface or interface region ($100\text{--}200\text{ nm}$) [77,78].

We, however, observe narrowing for both the overtone of the OH-stretching vibration $2\nu_{\text{OH}}$ ($\sim 6740\text{ cm}^{-1}$) and the $\nu_{\text{OH}} + \nu_2/\nu_{\text{OH}} + 2\nu_{\text{R}}$ combinational band ($\sim 5000\text{ cm}^{-1}$) in H ordered ice XIII, where H ordering is confirmed to be thermodynamically stable in the bulk from independent diffraction and DSC data [11,44].

The third signature for the presence of H order in ice XIII is the position and intensity of the combinational band of OH stretching, bending, and libration vibration ($\nu_{\text{OH}} + \nu_2 + \nu_{\text{R}}$) around $\sim 5500\text{ cm}^{-1}$. This band is blue-shifted by 33 cm^{-1} for ice XIII and less intense [Fig. 1(b) and Table I]. Note that this represents the first identification of H order based on intramolecular vibrations (OH-stretching and bending modes) that was previously thought to be insensitive to H ordering. In the past, it was thought that such differences manifest themselves merely in intermolecular lattice modes, e.g., librational or translational bands in the far infrared.

As pointed out by Moberg *et al.* [62,63], interpretation of the vibrational spectra of ices is far from trivial due to the strong intermolecular coupling and delocalization of vibrations within the H-bond network. They also point out that a straightforward assignment of symmetric and antisymmetric OH-stretching modes to certain bands falls short and that instead, bands are more likely composed of a mixture or, at best, a majority of one or the other molecular vibration mode. Thus, in their subsequent studies [62,63] (applying many-body molecular dynamics and normal mode calculations) they introduce indices for symmetry and localization. They find the low-wave number part of the OH-stretching band of ice XIII to consist of a majority of symmetric contributions (Figs. 5/6 in Ref. [63]). The high-wave number part of the OH-stretching band of ice XIII, however, is composed of an equal mixture of symmetric and antisymmetric contributions. We therefore tentatively expand their interpretation of the OH-fundamental band to the overtone band $2\nu_{\text{OH}}$ and hypothesize that the low-wave number shoulder of the $2\nu_{\text{OH}}$ band is composed of

mostly symmetric stretching modes. However, the effect of anharmonicity and increased peak separation favors distinction for vibrational overtones: The anharmonic contribution is different for H-ordered and H-disordered ices and causes differences in their vibrational signatures. The peak separation roughly doubles for the first overtone compared to the fundamental, which increases small differences to a level that can be recognized. Nevertheless, more experimental and computational work dedicated to the near-infrared spectrum of different hydrogen-ordered or -disordered ices shall be encouraged by the present Letter.

In summary, we here establish that near-infrared spectroscopy is an effective experimental method for probing H order in H₂O ices that is the first method also suitable for remote sensing experiments on ices in space. We tested the $2\nu_{\text{OH}}$ band for its applicability for astronomical observations by estimating observation times using the JWST Exposure Time Calculator [79]. Considering absorptivities similar to hexagonal ice [80] and fluxes similar to the ones observed toward the embedded protostar W33A [81,82], we estimate an exposure time of ~ 1 h using NIRSPEC at a fixed slit observation mode, using the G140H/F100LP disperser-filter combination with a resolving power of 2700 in order to achieve sufficient signal to noise ratios (>3) [83].

Based on the example of the ice XIII/V pair, we demonstrate that the spectral region of the first overtone of the OH-stretching vibration and the combinational bands around 5000 cm^{-1} and 5500 cm^{-1} can be used to differentiate ices which basically have the same oxygen network but only differ in their H lattice. More specifically, we observe splitting of the $2\nu_{\text{OH}}$ shoulder, narrowing of the $2\nu_{\text{OH}}$ and 5000 band, and a blueshift and shrinking of the $\nu_{\text{OH}} + \nu_2 + \nu_{\text{R}}$ combination band as signatures of hydrogen order. This represents the first intramolecular vibrational mode that allows for distinction between H order and H disorder or in other words for molecular orientations in ice crystals. Since orientations of water molecules are key for the electric and mechanical properties of ices as alluded to in the introduction, NIR sensing consequently also allows one to sense these properties remotely. So far, spectroscopic signatures of H order or H disorder have only been observed by Raman spectroscopy of isotopically mixed H₂O/D₂O ices in the intermolecular librational or translational region below $\sim 800\text{ cm}^{-1}$ [30,31], but not in the (near-)infrared $> 4000\text{ cm}^{-1}$, based on the overtone and combinational bands of the OH-stretching and bending vibration in isotopically pure H₂O ices, which is presented here for the first time. We show that NIR spectroscopy qualifies as a suitable method for scrutinizing H ordering in water ices both in the lab and in space, laying the foundation for directly testing the hypothesis of high-pressure H-ordered ices on the surface of celestial bodies by the near-infrared instruments on JWST and JUICE. The spectra of the pure ices reported here will then serve

the purpose as endmembers in spectroscopic modeling of ice and brine spectra collected by such instruments from icy bodies.

Acknowledgments—This research was supported by the Centre for Molecular Water Science (CMWS, DESY Hamburg) in an Early Science Project. C. M. T. received support from a DOC fellowship of the Austrian Academy of Sciences ÖAW and was supported by the Early Stage Funding 2021 of the University of Innsbruck. This research was funded in part by the Disruptive Innovation-Early Career Seed Money grant program of the Austrian Academy of Sciences (ÖAW) and the Austrian Science Fund (FWF). This research was funded in whole or in part by the Austrian Science Fund (FWF) [Grant-DOI 10.55776/PAT2619124].

-
- [1] T. Loerting, V. Fuentes-Landete, C. M. Tonaauer, and T. M. Gasser, Open questions on the structures of crystalline water ices, *Commun. Chem.* **3**, 1 (2020).
 - [2] T. Loerting, K. Winkel, M. Seidl, M. Bauer, C. Mitterdorfer, P. H. Handle, C. G. Salzmänn, E. Mayer, J. L. Finney, and D. T. Bowron, How many amorphous ices are there?, *Phys. Chem. Chem. Phys.* **13**, 8783 (2011).
 - [3] P. Ehrenfreund, H. J. Fraser, J. Blum, J. H. E. Cartwright, J. M. García-Ruiz, E. Hadamcik, A. C. Levasseur-Regourd, S. Price, F. Prodi, and A. Sarkissian, Physics and chemistry of icy particles in the Universe: Answers from microgravity, *Planet. Space Sci.* **51**, 473 (2003).
 - [4] J. D. Bernal and R. H. Fowler, A theory of water and ionic solution, with particular reference to hydrogen and hydroxyl ions, *J. Chem. Phys.* **1**, 515 (1933).
 - [5] P. Parkkinen, S. Riikonen, and L. Halonen, Ice XI: Not that ferroelectric, *J. Phys. Chem. C* **118**, 26264 (2014).
 - [6] H. Fukazawa, S. Ikeda, and S. Mae, Incoherent inelastic neutron scattering measurements on ice XI; The proton-ordered phase of ice I_h doped with KOH, *Chem. Phys. Lett.* **282**, 215 (1998).
 - [7] E. Whalley, J. B. R. Heath, and D. W. Davidson, Ice IX: An antiferroelectric phase related to ice III, *J. Chem. Phys.* **48**, 2362 (1968).
 - [8] W. B. Durham, S. H. Kirby, and L. A. Stern, Creep of water ices at planetary conditions: A compilation, *J. Geophys. Res.* **102**, 16293 (1997).
 - [9] T. Kubo, W. B. Durham, L. A. Stern, and S. H. Kirby, Grain size-sensitive creep in ice II, *Science* **311**, 1267 (2006).
 - [10] T. M. Gasser, A. V. Thoeny, A. D. Fortes, and T. Loerting, Structural characterization of ice XIX as the second polymorph related to ice VI, *Nat. Commun.* **12**, 1128 (2021).
 - [11] C. G. Salzmänn, P. G. Radaelli, A. Hallbrucker, E. Mayer, and J. L. Finney, The preparation and structures of hydrogen ordered phases of ice, *Science* **311**, 1758 (2006).
 - [12] B. Kamb, A. Prakash, and C. Knobler, Structure of ice. V, *Acta Crystallogr.* **22**, 706 (1967).
 - [13] B. Kamb, W. C. Hamilton, S. J. LaPlaca, and A. Prakash, Ordered proton configuration in ice II, from single-crystal neutron diffraction, *J. Chem. Phys.* **55**, 1934 (1971).

- [14] B. Kamb and A. Prakash, Structure of ice III, *Acta Crystallogr. Sect. B* **24**, 1317 (1968).
- [15] H. Engelhardt and B. Kamb, Structure of ice IV, a metastable high-pressure phase, *J. Chem. Phys.* **75**, 5887 (1981).
- [16] S. J. La Placa, W. C. Hamilton, B. Kamb, and A. Prakash, On a nearly proton-ordered structure for ice IX, *J. Chem. Phys.* **58**, 567 (1973).
- [17] B. Kamb, Structure of ice VI, *Science* **150**, 205 (1965).
- [18] J. D. Jorgensen, R. A. Beyerlein, N. Watanabe, and T. G. Worlton, Structure of D₂O ice VIII from *in situ* powder neutron diffraction, *J. Chem. Phys.* **81**, 3211 (1984).
- [19] B. Kamb and B. L. Davis, Ice VII, the densest form of ice, *Proc. Natl. Acad. Sci. U.S.A.* **52**, 1433 (1964).
- [20] C. Lobban, J. L. Finney, and W. F. Kuhs, The structure of a new phase of ice, *Nature (London)* **391**, 268 (1998).
- [21] C. G. Salzmann, P. G. Radaelli, E. Mayer, and J. L. Finney, Ice XV: A new thermodynamically stable phase of ice, *Phys. Rev. Lett.* **103**, 105701 (2009).
- [22] A. Falenty, T. C. Hansen, and W. F. Kuhs, Formation and properties of ice XVI obtained by emptying a type SII clathrate hydrate, *Nature (London)* **516**, 231 (2014).
- [23] L. del Rosso, M. Celli, D. Colognesi, F. Grazzi, and L. Ulivi, Irreversible structural changes of recovered hydrogen hydrate transforming from C0 phase to ice XVII, *Chem. Phys.* **544**, 111092 (2021).
- [24] J. M. Besson, M. Kobayashi, T. Nakai, S. Endo, and P. Pruzan, Pressure dependence of Raman linewidths in ices VII and VIII, *Phys. Rev. B* **55**, 11191 (1997).
- [25] M. Celli, L. Ulivi, and L. del Rosso, Raman investigation of the Ice I_c – Ice I_h transformation, *J. Phys. Chem. C* **124**, 17135 (2020).
- [26] C. Salzmann, I. Kohl, T. Loerting, E. Mayer, and A. Hallbrucker, The Raman spectrum of ice XII and its relation to that of a new “high-pressure phase of H₂O ice”, *J. Phys. Chem. B* **106**, 1 (2002).
- [27] M. J. Taylor and E. Whalley, Raman spectra of ices I_h, I_c, II, III, and V, *J. Chem. Phys.* **40**, 1660 (1964).
- [28] A. K. Garg, High-pressure Raman spectroscopic study of the ice I_h → ice IX phase transition, *Phys. Status Solidi (a)* **110**, 467 (1988).
- [29] B. Minceva-Sukarova, W. F. Sherman, and G. R. Wilkinson, The Raman spectra of ice (I_h, II, III, V, VI and IX) as functions of pressure and temperature, *J. Phys. C* **17**, 5833 (1984).
- [30] T. Shigenari and K. Abe, Vibrational modes of hydrogens in the proton ordered phase XI of ice: Raman spectra above 400 cm⁻¹, *J. Chem. Phys.* **136**, 174504 (2012).
- [31] C. G. Salzmann, A. Hallbrucker, J. L. Finney, and E. Mayer, Raman spectroscopic study of hydrogen ordered ice XIII and of its reversible phase transition to disordered ice V, *Phys. Chem. Chem. Phys.* **8**, 3088 (2006).
- [32] A. V. Thoeny, T. M. Gasser, and T. Loerting, Distinguishing ice β-XV from deep glassy ice VI: Raman spectroscopy, *Phys. Chem. Chem. Phys.* **21**, 15452 (2019).
- [33] P. T. T. Wong, Raman spectrum of ice VIII, *J. Chem. Phys.* **64**, 2359 (1976).
- [34] Y. Yoshimura, S. T. Stewart, M. Somayazulu, H. K. Mao, and R. J. Hemley, Convergent Raman features in high density amorphous ice, ice VII, and ice VIII under pressure, *J. Phys. Chem. B* **115**, 3756 (2011).
- [35] M. Arakawa, H. Kagi, and H. Fukazawa, Laboratory measurements of infrared absorption spectra of hydrogen-ordered ice: A step to the exploration of ice XI in space, *Astrophys. J. Suppl. Ser.* **184**, 361 (2009).
- [36] T. F. Whale, S. J. Clark, J. L. Finney, and C. G. Salzmann, DFT-assisted interpretation of the Raman spectra of hydrogen-ordered ice XV: Raman spectra of hydrogen-ordered ice XV, *J. Raman Spectrosc.* **44**, 290 (2013).
- [37] M. Arakawa and H. Kagi, Erratum: “Laboratory measurements of infrared absorption spectra of hydrogen-ordered ice: A step to the exploration of ice XI in space” (2009, ApJS, 184, 361), *Astrophys. J. Suppl. Ser.* **246**, 18 (2020).
- [38] S. Vance, M. Bouffard, M. Choukroun, and C. Sotin, Ganymede’s internal structure including thermodynamics of magnesium sulfate oceans in contact with ice, *Planet. Space Sci.* **96**, 62 (2014).
- [39] M. G. Kivelson, K. K. Khurana, and M. Volwerk, The permanent and inductive magnetic moments of Ganymede, *Icarus* **157**, 507 (2002).
- [40] C. Sotin and G. Tobie, Internal structure and dynamics of the large icy satellites, *C.R. Phys.* **5**, 769 (2004).
- [41] J. S. Kargel, J. Z. Kaye, J. W. Head, G. M. Marion, R. Sassen, J. K. Crowley, O. P. Ballesteros, S. A. Grant, and D. L. Hogenboom, Europa’s crust and ocean: Origin, composition, and the prospects for life, *Icarus* **148**, 226 (2000).
- [42] R. Pozzobon, G. Cremonese, M. Capria, V. Da Deppo, and M. Massironi, *Analysis of Tectonics and Cryovolcanism on Ganymede: Possible Observations with JGO-EJSM* (2011), Vol. 2011, p. 1019, <https://meetingorganizer.copernicus.org/EPSC-DPS2011/EPSC-DPS2011-1019-1.pdf>.
- [43] N. Ligier, C. Paranicas, J. Carter, F. Poulet, W. M. Calvin, T. A. Nordheim, C. Snodgrass, and L. Ferellec, Surface composition and properties of Ganymede: Updates from ground-based observations with the near-infrared imaging spectrometer SINFONI/VLT/ESO, *Icarus* **333**, 496 (2019).
- [44] C. G. Salzmann, P. G. Radaelli, J. L. Finney, and E. Mayer, A calorimetric study on the low temperature dynamics of doped ice V and its reversible phase transition to hydrogen ordered ice XIII, *Phys. Chem. Chem. Phys.* **10**, 6313 (2008).
- [45] K. Yamashita and T. Loerting, Thermodynamically stable intermediate in the course of hydrogen ordering from ice V to ice XIII, *J. Phys. Chem. Lett.* **15**, 1181 (2024).
- [46] C. M. Tonauer, K. Yamashita, L. D. Rosso, M. Celli, and T. Loerting, Enthalpy change from pure cubic ice I_c to hexagonal Ice I_h, *J. Phys. Chem. Lett.* **14**, 5055 (2023).
- [47] K. W. Köster, A. Raidt, V. Fuentes Landete, C. Gainaru, T. Loerting, and R. Böhmer, Doping-enhanced dipolar dynamics in ice V as a precursor of hydrogen ordering in ice XIII, *Phys. Rev. B* **94**, 184306 (2016).
- [48] J. E. Bertie, H. J. Labbé, and E. Whalley, Absorptivity of ice I in the range 4000–30 cm⁻¹, *J. Chem. Phys.* **50**, 4501 (1969).
- [49] J. E. Bertie and E. Whalley, Infrared spectra of ices I_h and I_c in the range 4000 to 350 cm⁻¹, *J. Chem. Phys.* **40**, 1637 (1964).
- [50] J. E. Bertie, L. D. Calvert, and E. Whalley, Transformations of ice II, ice III, and ice V at atmospheric pressure, *J. Chem. Phys.* **38**, 840 (1963).

- [51] H. Engelhardt and E. Whalley, The infrared spectrum of ice IV in the range 4000–400 cm^{-1} , *J. Chem. Phys.* **71**, 4050 (1979).
- [52] J. E. Bertie, H. J. Labbé, and E. Whalley, Infrared spectrum of ice VI in the range 4000–50 cm^{-1} , *J. Chem. Phys.* **49**, 2141 (1968).
- [53] J. E. Bertie and S. M. Jacobs, Far-infrared absorption by ices I_h and I_c at 4.3 °K and the powder diffraction pattern of ice I_c , *J. Chem. Phys.* **67**, 2445 (1977).
- [54] J. E. Bertie, H. J. Labbé, and E. Whalley, Far-infrared spectra of ice II, V, and IX, *J. Chem. Phys.* **49**, 775 (1968).
- [55] T. L. C. Jansen, S. Saito, J. Jeon, and M. Cho, Theory of coherent two-dimensional vibrational spectroscopy, *J. Chem. Phys.* **150**, 100901 (2019).
- [56] H. Tran, A. V. Cunha, J. J. Shephard, A. Shalit, P. Hamm, T. L. C. Jansen, and C. G. Salzmann, 2D IR spectroscopy of high-pressure phases of ice, *J. Chem. Phys.* **147**, 144501 (2017).
- [57] F. Perakis and P. Hamm, Two-dimensional infrared spectroscopy of neat ice I_h , *Phys. Chem. Chem. Phys.* **14**, 6250 (2012).
- [58] F. Perakis, S. Widmer, and P. Hamm, Two-dimensional infrared spectroscopy of isotope-diluted ice I_h , *J. Chem. Phys.* **134**, 204505 (2011).
- [59] F. Perakis, J. A. Borek, and P. Hamm, Three-dimensional infrared spectroscopy of isotope-diluted ice I_h , *J. Chem. Phys.* **139**, 014501 (2013).
- [60] T. Begušić and G. A. Blake, Two-dimensional infrared-Raman spectroscopy as a probe of water’s tetrahedrality, *Nat. Commun.* **14**, 1950 (2023).
- [61] L. Shi, J. L. Skinner, and T. L. C. Jansen, Two-dimensional infrared spectroscopy of neat ice I_h , *Phys. Chem. Chem. Phys.* **18**, 3772 (2016).
- [62] D. R. Moberg, S. C. Straight, C. Knight, and F. Paesani, Molecular origin of the vibrational structure of ice I_h , *J. Phys. Chem. Lett.* **8**, 2579 (2017).
- [63] D. R. Moberg, P. J. Sharp, and F. Paesani, Molecular-level interpretation of vibrational spectra of ordered ice phases, *J. Phys. Chem. B* **122**, 10572 (2018).
- [64] L. Shi, S. M. Gruenbaum, and J. L. Skinner, Interpretation of IR and Raman line shapes for H_2O and D_2O ice I_h , *J. Phys. Chem. B* **116**, 13821 (2012).
- [65] L. Shi and J. L. Skinner, Proton disorder in ice I_h and inhomogeneous broadening in two-dimensional infrared spectroscopy, *J. Phys. Chem. B* **117**, 15536 (2013).
- [66] J. M. Bowman, Y. Wang, H. Liu, and J. S. Mancini, *Ab initio* quantum approaches to the IR spectroscopy of water and hydrates, *J. Phys. Chem. Lett.* **6**, 366 (2015).
- [67] R. Escribano, P. C. Gómez, B. Maté, G. Molpeceres, and E. Artacho, Prediction of the near-IR spectra of ices by *ab initio* molecular dynamics, *Phys. Chem. Chem. Phys.* **21**, 9433 (2019).
- [68] M. J. Wójcik, M. Gług, M. Boczar, and Ł. Boda, Spectroscopic signature for ferroelectric ice, *Chem. Phys. Lett.* **612**, 162 (2014).
- [69] Y. Langevin and G. Piccioni, MAJIS (Moons And Jupiter Imaging Spectrometer) for JUICE: Objectives for the Galilean satellites, in European Planetary Science Congress (2013), Vol. **8**, p. 548-1, <https://meetingorganizer.copernicus.org/EPSC2013/EPSC2013-548-1.pdf>.
- [70] C. M. Tonauer, E.-M. Köck, T. M. Gasser, V. Fuentes-Landete, R. Henn, S. Mayr, C. G. Kirchler, C. W. Huck, and T. Loerting, Near-infrared spectra of high-density crystalline H_2O ices II, IV, V, VI, IX, and XII, *J. Phys. Chem. A* **125**, 1062 (2021).
- [71] C. M. Tonauer, M. Seidl-Nigsch, and T. Loerting, High-density amorphous ice: Nucleation of nanosized low-density amorphous ice, *J. Phys. Condens. Matter* **30**, 034002 (2018).
- [72] See Supplemental Material at <http://link.aps.org/supplemental/10.1103/x2ph-yp2v> for more details.
- [73] C. G. Salzmann, I. Kohl, T. Loerting, E. Mayer, and A. Hallbrucker, The low-temperature dynamics of recovered ice XII as studied by differential scanning calorimetry: A comparison with ice V, *Phys. Chem. Chem. Phys.* **5**, 3507 (2003).
- [74] Y. Tajima, T. Matsuo, and H. Suga, Phase transition in KOH-doped hexagonal ice, *Nature (London)* **299**, 810 (1982).
- [75] T. Sugimoto, N. Aiga, Y. Otsuki, K. Watanabe, and Y. Matsumoto, Emergent high- T_c ferroelectric ordering of strongly correlated and frustrated protons in a heteroepitaxial ice film, *Nat. Phys.* **12**, 1063 (2016).
- [76] M. Arakawa, H. Kagi, J. A. Fernandez-Baca, B. C. Chakoumakos, and H. Fukazawa, The existence of memory effect on hydrogen ordering in ice: The effect makes ice attractive: Memory effect on H-ordering in ice, *Geophys. Res. Lett.* **38**, L16101 (2011).
- [77] K. Kobayashi and H. Yasuda, Phase transition of ice I_c to ice XI under electron beam irradiation, *Chem. Phys. Lett.* **547**, 9 (2012).
- [78] A. Kouchi *et al.*, UV-induced formation of ice XI observed using an ultra-high vacuum cryogenic transmission electron microscope and its implications for planetary science, *Front. Chemistry* **9**, 799851 (2021).
- [79] K. M. Pontoppidan *et al.*, Pandeia: A multi-mission exposure time calculator for JWST and WFIRST, in *Observatory Operations: Strategies, Processes, and Systems VI*, edited by A. B. Peck, C. R. Benn, and R. L. Seaman (SPIE, Edinburgh, United Kingdom, 2016), Vol. 9910, p. 44, 10.1117/12.2231768.
- [80] S. G. Warren and R. E. Brandt, Optical constants of ice from the ultraviolet to the microwave: A revised compilation, *J. Geophys. Res.* **113**, D14220 (2008).
- [81] R. Capps, F. Gillett, and R. Knacke, Infrared observations of the OH source W33 A: Part 1, *Astrophys. J.* **226**, 863 (1978).
- [82] E. L. Gibb *et al.*, An inventory of interstellar ices toward the embedded protostar W33A, *Astrophys. J.* **536**, 347 (2000).
- [83] P. D. Tribbett, S. C. Tegler, and M. J. Loeffler, Probing microporous ASW with near-infrared spectroscopy: Implications for JWST’s NIRSpec, *Astrophys. J.* **915**, 40 (2021).